High Duty Cycle (HDC) Sonar Processing Interval and Bandwidth Effects for the TREX'13 Dataset

Randall Plate, Doug Grimmett
SPAWAR Systems Center Pacific
San Diego, CA, USA
rplate@spawar.navy.mil, grimmett@spawar.navy.mil

***Abstract*— Unlike conventional Pulsed Active Sonar (PAS), which listens for target echoes in between short-burst transmissions, High Duty Cycle (HDC) sonar attempts to detect echoes amidst the continual interference from source(s) transmitting with nearly 100% duty cycle. HDC sonar presents an additional processing parameter, not available with PAS, which is the processing interval. The processing interval is a selectable subset of time within a CAS repetition cycle used for coherent processing. Hence, the choice of processing interval may be used to tune the performance of the sonar to local environmental conditions and to the operational scenario. Theoretically, increasing the processing interval increases target detectability, but in practice other factors should also be considered. In real acoustic environments, sound propagation is subject to temporal and spectral spreading effects, and these may limit the processing gains to lower levels than expected. Target Doppler can also become a more significant issue with longer processing intervals. Shorter processing intervals provide an increased number and rate of detection opportunities, which can be a significant advantage, leading to improved target holding, localization, tracking, and classification.**

This paper describes the various expected effects of the processing interval on performance for continuous-time LFM signals. It presents an analysis conducted on the TREX'13 sea trial dataset, and shows various results achieved as a function of processing interval. The results are explained and compared with theoretical expectations, and show the complicating effects of a real acoustic environment. In particular, we see the limitation on performance gains with increasing the processing interval due to acoustic environmental spreading effects, the target's physical extent and Doppler effects. Comparisons are shown between echoes from three different targets: mobile compact, mobile extended, and fixed. The evaluation describes performance using the quantities of Received Level, SNR, echo time-extent, and delay bias.

Keywords— continuous active sonar; high duty cycle sonar; continuous time LFM

I. INTRODUCTION

Recently, there has been emerging interest in the concept of High Duty Cycle (HDC) Sonar. Unlike Pulsed Active Sonar (PAS), which listens for echoes in between short transmission bursts, HDC sonar attempts to detect echoes amidst the continual interference from source(s) transmitting with nearly 100% duty cycle. A schematic of the two contrasting approaches is shown in Fig. 1. A potential advantage of HDC sonar is an increased number of continuous detection opportunities, leading to improved target detection, localization, tracking, and classification. In addition, lower transmission source levels are possible. Of course, appropriate HDC-specific processing must be employed to enable detection in the presence of continuous transmissions. The HDC concept can be implemented within monostatic or multistatic systems, though in the case of multistatic systems the additional challenges of multisource mutual interference and effective data fusion must be overcome.

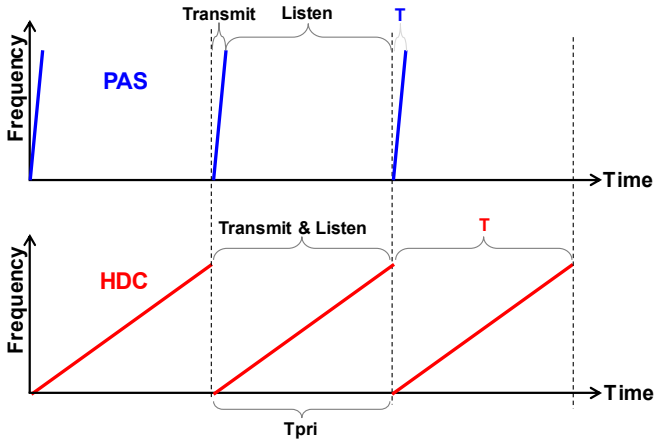

Fig. 1. Depiction of three cycles of PAS (top, blue) and HDC (bottom, red) transmission methods. The PAS "listens after transmit" and the HDC method "listens while transmit". T_{pri} is the ping repetition interval and T is the LFM signal duration.

Like PAS systems, HDC sonar systems may employ a variety of signal types. Single FM waveforms provide good target ranging measurements, but no Doppler information. Alternatively, CW waveforms provide good target Doppler (range-rate) measurements, but no ranging information. Systems, including multistatic systems, can gain valuable geometrically complementary detection opportunities when both signal types are used [1]. Finally, one may consider broadband waveforms which attempt to provide both good range and Doppler measurements simultaneously [2].

An HDC system which solely employs CW waveforms is unable to estimate target range, unless detections from multiple sensors (e.g., within multistatic configurations) are fused. These may be utilized for cross-fixing within a target tracker to obtain an unambiguous geographic localization [3]. An HDC system which employs the FM waveform provides unambiguous target range measurements. Furthermore, unlike

a PAS system, it can provide multiple detection opportunities within a single ping repetition interval or cycle (T_{pri}), when the longer HDC LFM received signals are broken up and processed in shorter time blocks. Though the probability of detection and ranging accuracy may be lower for shorter processing intervals, a distinct advantage is that there is a shorter time lapse between measurements. This allows near continuous holding on a target and reduced growth of its area of uncertainty (AOU) [4]. This can improve target localization, holding, maneuver detection, and false track rate.

LFM signals suffer from the well-known range (or time-delay) bias error problem [5]. This bias error is a function of operating frequency, waveform frequency-time sweep rate, and the apparent target Doppler. Because HDC LFM signals have a slower sweep-rate than PAS LFM signals, they will have significantly larger bias errors. The problem is exacerbated when transmission system bandwidth is limited or small. For single sensor systems, range biases will simply cause a tracker to mis-localize the target. In the case of a multistatic system, different range biases on the various sensors may be severe enough to prevent data association (gating) and effective fusion of the information, resulting in degraded tracker output.

Systems utilizing only FM signals are unable to directly measure target Doppler. Velocity estimates are only obtained through a multi-ping observation of the change in target range (range-rate). In PAS systems, the measurement update interval corresponds to the ping repetition interval, so reliable range-rate estimation may take some time to obtain. In addition, if the target quickly maneuvers over that time it may be difficult to establish track or to follow it. With HDC LFM signals, the update rate can be much quicker, with many potential target observations within a single T_{pri} [6], and enable better Doppler estimates in less time from FM signals.

The remainder of this paper is as follows. HDC LFM signals are described in Section II. Sections III and IV describe the theoretically expected performance as a function of processing interval/bandwidth and Doppler, respectively. Section V describes the TREX'13 seatrial data collection and section VI presents the results of analysis on that data. Section VII provides a summary and conclusions.

II. Continuous Active Sonar using LFM Signals

The LFM signal is one in which the instantaneous frequency is "swept" linearly over time. The signals can be swept up ("upsweeps") or down ("downsweeps"). LFM signals are convenient for HDC operations because time delay is straightforwardly extracted from measurements of Doppler shift. The equation for an LFM signal is given by:

$$s_{FM}(t) = \sqrt{\frac{2}{T}} \cdot cos\left[2\pi\left(f_1 t + k\frac{t^2}{2}\right)\right]; \quad -\frac{T}{2} \le t \le \frac{T}{2}, \quad (1)$$

where the frequency-time slope (or sweep rate) is given by

$$k = \frac{f_2 - f_1}{T} = \frac{B}{T}, \quad (2)$$

where T is the LFM signal duration, f_1 is the sweep start frequency, f_2 is the sweep stop frequency, and B is the bandwidth. The instantaneous frequency is given by the derivative of the signal's phase term as $f = f_1 + kt$.

A continuous-time LFM (CTLFM) extends the duration of the LFM over the entire ping repetition cycle (T_{pri}) and repeats. Fig. 2 depicts a CTLFM waveform with total bandwidth B, and a duration T_{pri}. The echo from a target arrives with time delay, $\Delta\tau$, which may be obtained via two different, but equivalent, processing methods. One method employs temporal processing; i.e., matched filtering of the data. This is done by splitting the total signal bandwidth into a selectable number of frequency sub-bands, each of bandwidth B_p, corresponding to processing time T_p, and then processing them with a bank of matched filters. Alternatively, the received signal may be heterodyned (de-chirped) and processed spectrally [7], with the relationships:

$$\Delta\tau = \Delta f \cdot \frac{T_{pri}}{B}; \quad B_p = kT_p \quad (3)$$

where Δf is the echo's frequency shift. The analysis done here will use the matched filter processing method, which is a more straightforward implementation.

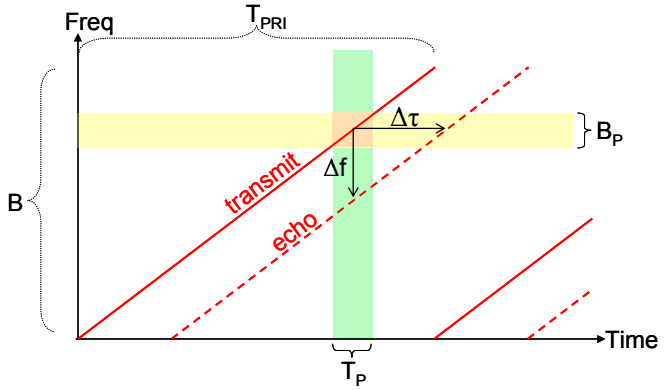

Fig. 2. Depiction of an example LFM signal in amplitude and frequency vs. time. Yellow indicates the temporal procesing method and the green indicates the sprectral processing method.

III. Performance vs. Processing Time/Bandwidth

HDC signal processing may be done on smaller sub-sections (in time and frequency) of the full LFM waveform. This can provide more detection opportunities; however, they may be somewhat degraded in terms of amplitude and accuracy compared to processing with the full LFM bandwidth. The LFM range resolution is approximately given by

$$\Delta r \approx \frac{c}{2B_p}, \quad (4)$$

where c is the speed of sound in water. So, processing smaller time-bandwidth segments at faster update rates will decrease measurement resolution. The impact of this is twofold: first, the decrease in resolution means more uncertainty in the target's localized position; second, echo signal-to-background level may be reduced.

Some sectors of the surveillance space may be limited by reverberation; others may be limited by noise. Reductions in T_p and B_p will lead to larger observation cells in range and Doppler, respectively. Within these larger cells, more noise or reverberation will enter and raise the acoustic level measured in the cell. This results in a loss in the echo-to-background level and decreased detectability. The theoretical signal processing gains against background noise and reverberation cases are given as

$$PG_{noise} \sim 10 * log_{10}(T_p) = 10 \cdot log_{10}(T/N), \quad (5)$$

$$PG_{reverb} \sim 10 * log_{10}(B_p) = 10 \cdot log_{10}(B/N), \quad (6)$$

where *N* is the number of sub-bands the full waveform cycle is broken into for processing. Therefore, doubling the processing time should provide about a 3 dB gain against noise, while doubling bandwidth should provide a similar 3 dB gain against reverberation. However, this assumes that the acoustic channel is completely coherent in time and frequency, over the entire time/frequency band being processed, which is typically not the case for real underwater acoustic environments.

Many propagation channels, and acoustic channels in particular, are subject to extreme time spreading and frequency spreading which destroy temporal and spectral coherence of signal propagation. In this case, processing larger time/frequency bands beyond the limits which the channel is coherent over will not provide the expected theoretical increase in gain. Knowing the channel coherence limits enables the system designer to make suitable choices for processing.

The temporal spreading losses for target echoes may be due to several factors:

- The target itself is not normally a point target. Instead it will have some physical dimensions and aspect angle presented to the sonar which will cause the target echo energy to be spread out in time corresponding to these dimensions.
- The target may be mobile and if so, it will be continuously ensonified as it moves along its trajectory. This is less of an issue for PAS, but for HDC the issue is significant due to the low sweep-rate. It results in increased temporal echo spreading corresponding to the range change of the target over the processing interval. Of course, the faster the target speed, the more this effect will be. This effect may be avoided if Dopplerized LFM replicas (or Dopplerized heterodyning) are implemented.
- Underwater acoustic channels are notoriously complicated, and are typically characterized by severe multipath propagation. This effect is exacerbated in shallow water environments where there are many interactions with highly refractive channel and reflections from the bottom and surface boundaries. Therefore the target's echo itself will be spread by the environment, independent of the target.

Frequency spreading of target echoes may also occur. The target may have a non-constant velocity along its trajectory. Or, the apparent velocity to the sonar may vary over the processing interval due to the projection of the velocity to the viewpoint of the sonar. Environmental effects will also cause frequency spreading. This is likely to be driven by an undulating, rough sea surface, from which many echo sound paths will be reflected. There may also be spreading effects due to currents and/or internal waves.

IV. DOPPLER PROCESSING

When mobile targets are present, Doppler-compensated LFM replicas may be used to improve detection performance. The frequency shifts are obtained by time-scaling replicas to match the hypothesized Doppler shifts. For PAS LFM signals this is typically neglected because Doppler effects are negligible due to the short length of the waveform. For HDC sonar, the longer processing times will necessitate consideration of this.

Doppler mismatch between the received echoes and matched filter replicas results in three degradations to processed correlations: increased peak width, reduced peak amplitude, and time delay bias. These three effects can be predicted by computing the ambiguity surface for a given waveform.

Fig. 3 shows these surfaces for five different processing time/bandwidth cases of the LFM waveform used in the data analysis presented later. The slanted ridge indicates time bias error that increases (from zero delay bias) with increased target Doppler. It is observed that, in general, shorter processing times spread the peak energy out in the time delay dimension, reducing overall peak height. Increasing time-bandwidth product results in narrowing the peak, and thereby increasing the maximum height. However, at T_p = 9 we start to clearly see another phenomenon – that the sensitivity to Doppler mismatch increases and results in a fanning of the pulse width out from the center of the surface. Therefore, the longest processing time (T_p = 18) has a very sharp peak at 0 Doppler mismatch, but has the potential for a wider peak than does, for example, T_p = 4 sec, which has only a moderately wide peak over a wide range of Doppler.

The time delay bias is determined by

$$\tau = \frac{2\dot{r}f}{ck} \quad (7)$$

where $\dot{r}$ is the range rate of the target, and f is the center frequency of the processed pulse. Thus, since k is constant for subbands of the LFM waveform, the slope of the ridge in the ambiguity function is independent of subband. It is, however, dependent on the frequency band of the processed waveform. Additionally, due to this slope, each sub-band, will have a different bias, leading to a variable arrival-time "sawtooth" pattern over cycles, which may be exploited to ascertain target Doppler even when Doppler processing is not done [6].

A representative PAS waveform utilizing the entire bandwidth, but with only a one second duration, is also shown for comparison. This waveform will obviously have a much larger value of k, resulting in significantly reduced bias over the same range of Dopplers, in addition to narrower pulse width. Hence, in this case LFM Doppler processing is normally not required.

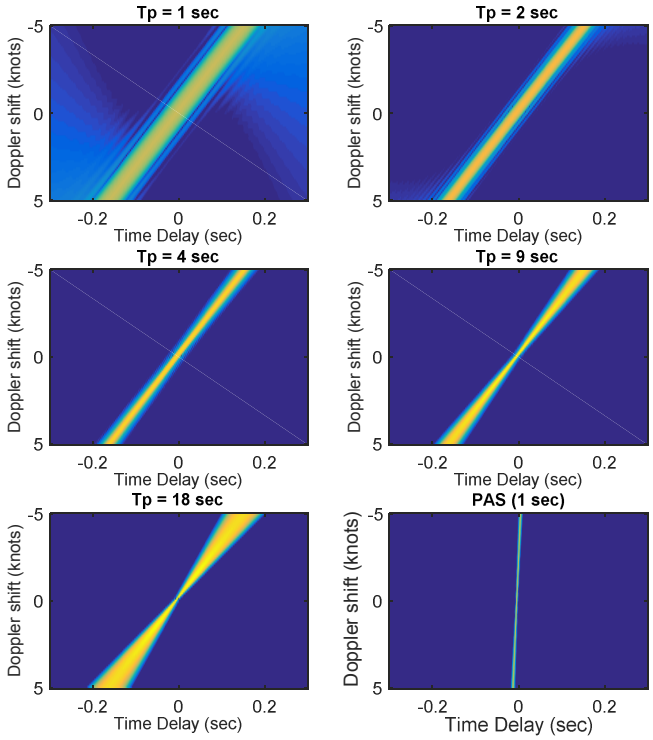

Fig. 3. Ambiguity surfaces for LFM signal for various HDC subbands and a PAS waveform.

V. THE TREX'13 SEATRIAL DATA

The TREX'13 sea trial [8] was conducted during May, 2013, off the coast of Panama City, Florida. This trial was a collaborative effort between ONR, APL/UW, and DRDC-Atlantic. The HDC portion of the experiment utilized a fixed, bottom-moored acoustic source and hydrophone line array in a nearly monostatic configuration. These were operated by the R.V. SHARP, which was moored nearby and collected the receiver data. The trial was situated in an extremely shallow area with water depths of about 10-12 meters. The target was provided by DRDC-Atlantic, and consisted of the SMART Echo Repeater (E/R) system towed by the Canadian vessel CFAV Quest, which provided a way to simulate an actual submarine target. Track trajectories were run radially inbound and outbound from the monostatic sonar, over ranges of 10-15 km.

For this analysis we have focused on Run 80 of the experiment. The source transmitted an unshaded upsweep LFM signal of 18-second duration over the frequency band of 1800-2700 Hz. The signal was continuously repeated, but with a two-second (non-transmitting) gap between each cycle ($T = 18\ s, T_{pri} = 20\ s$). The Quest maintained an outbound radial trajectory at a speed of 5 kts, with the E/R operating in a "ping pong" mode that captured every odd-numbered source transmission ping cycle and then retransmitted it on every even-numbered transmitted cycle with an amplified level of 0 dB (Target Strength). In this manner E/R echoes were obtained on the receiver every other ping cycle with the correct echo timing. Run 80 was one hour in duration; we focus our analysis on the first 30 minutes of the run.

The received data were beamformed (during Run 80 the target was always within a single beam) and then processed using a bank of matched filters to cover the entire signal bandwidth (1800 Hz) with sub-bands corresponding to processing intervals, T_p, of 1, 2, 4, 9, and 18 seconds as shown in Table I. The matched filtered data was processed using a split window normalizer, and a detection threshold was applied. Detection "contacts" were extracted with the following information: echo time, echo received level, echo signal-to-background level, and echo time extent.

Fig. 4 shows the processed output for the entire 30 minutes for case 5 (T_p =18 s, B_p=50 Hz). The output of each matched filter in the bank is time-aligned so that echo delays can be compared from processing interval to processing interval. The direct blast arrivals are seen at 0 seconds, with the echoes of the following three targets highlighted:

- E/R echoes: These occurred every other transmission cycle. This target can be considered a compact "point" target, with very limited physical dimensions (small hydrophone and projector). It was mobile, being towed from the Quest, and therefore contains motion and Doppler effects. These echoes will be slightly delayed in time relative to the HULL echoes.
- HULL echoes: There was sufficient energy ensonifying and reflecting from the hull of the Quest surface ship. This target had a length of 72 m, and therefore we expect it to be more temporally distributed than the echo repeater target. It also manifests all the expected motion and Doppler effects.
- HOSE echoes: A fixed, moored, air-filled tube was deployed in the area. It served as a high strength, point-like target. The target can be considered a stationary, fixed target without any motion or Doppler effects. Since it extends vertically throughout the water column, it has limited target (physical) extent for temporal spreading considerations.

The Hull and E/R echoes are observed increasing in delay time as run time progresses due to the Quest traveling directly away from the source; the Hose was stationary for the duration of the run. The next section will present analysis and comparisons of the echoes from these three targets as functions of processing interval.

TABLE I. TREX'13 PROCESSING BANDS

	Processing time T_p (s)	**Processing bandwidth B_p (Hz)**	**Number of sub-bands N**	**Total number of detection opportunities**
Case 1	18	900	1	90
Case 2	9	450	2	180
Case 3	4	200	4	360
Case 4	2	100	9	810
Case 5	1	50	18	1620

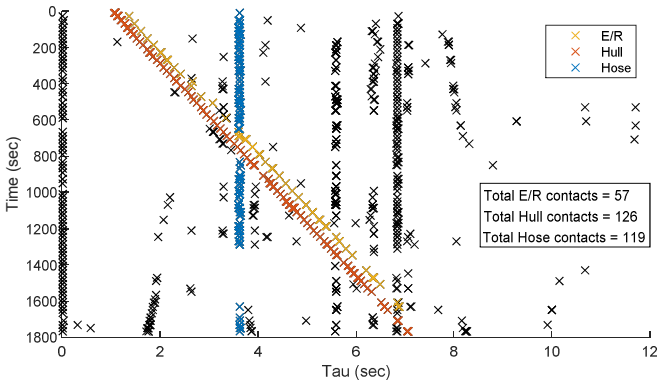

Fig. 4. Example output of processed result.

VI. TREX'13 Data Analysis

Statistics were automatically computed to investigate trends in the data as functions of processing time/bandwidth. In addition, a subset of contacts from specific scans have been extracted by hand and analyzed to estimate certain parameters that were challenging to automate. Background levels were difficult to estimate automatically due to the close proximity of multiple targets and other clutter objects generating peaks that interfered with the measurements. Peak widths were difficult to calculate automatically due to the variations in peaks. These specific scans (14, 26, 30, 36, 48, and 54) were selected because they contained strong detections on all three targets.

As listed in Table I, five sub-bands were processed, varying from the full waveform (18 sec) down to 1 sec, and chosen to be roughly factors of two apart. Due to the structure of the LFM waveform, sub-bands scale processing time and bandwidth at the same ratio, thus doubling of T_p also mandates a doubling of B_p, and results are shown as a function of these. Fig. 5 shows A-scans of each of the sub-bands processed for scan 26 of the data (the 26th transmitted sweep, which occurred 500 seconds into the run). This example captures the time near when the Quest crossed over the fixed air hose and thus all three targets are shown in close proximity.

The data were match-filtered with two replicas: one with no Doppler correction (same as the transmitted waveform) for processing the fixed Hose target, and one that was corrected for a 5-knot opening target for processing the Hull and E/R targets. For analysis purposes we consider contacts that are "Doppler-matched" (the Air Hose in the left column, and the Hull and E/R in the right column) and those that are "Doppler-mismatched" (Hull and E/R in the left column, and Air Hose in the right). Two of the three primary degradations due to Doppler mismatch, reduced peak amplitude and increased peak width, are clearly observable comparing the detections in the left and right columns of Fig. 5; these effects will also be illustrated in the subsequent sections in more detail. The Doppler bias error is also present for the mismatched targets, but not intuitively apparent, and will be discussed in more detail in subsection *E*. Note that the matched filter correlations are normalized to obtain constant peak level across processing times, with drops in background levels observed as processing times (correlation lengths) increase. Resolution is also seen to increase as processing time increases.

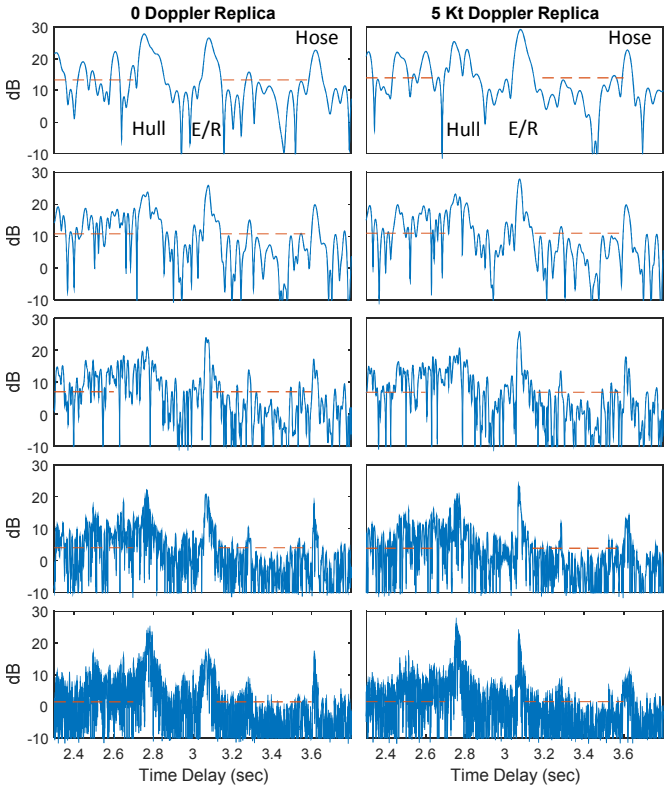

Fig. 5. Matched filter outputs for scan #26 as a function of T_p (1,2,4,9,18 sec, from top to bottom); zero kt replica (left) and 5 kt Doppler replica (right).

For the hand analysis, the background reverb levels were estimated by averaging over data segments left and right of the target peaks; the calculated background levels and averaging regions used for the Hull and E/R are shown by red lines.

Fig. 6 shows smoothed (moving-average) acoustic background levels as a function of time delay (equivalent to target range) near the beginning of the run (scan 5) and the end of the run (scan 175). For each scan, processing with a short sub-band (T_p = 1 sec) and full band (T_p = 18 sec) are shown, with the full band being approximately 12 dB lower due to processing gain, as will be explained in subsection *D*. The transition from the reverb-limited region to the noise-limited region can be seen around 7 to 9 seconds of delay. A reduction

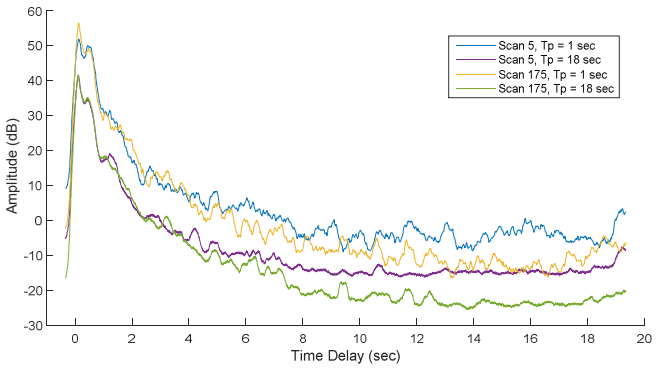

Fig. 6. Average acoustic levels vs. time delay for small vs. large sub-bands at beginning and end of run.

in background noise is observed from scan 5 to scan 175, indicating a change in the environment over this time frame, while the reverberation levels are the same at the beginning and end of the run, as is expected. Note that the data shown in Fig. 5 is in the sloping reverb-limited region, and hence the background floor is higher for the Hull and E/R than the Hose.

A. Matched Filter Resolution

The most apparent difference between the five cases shown in Fig. 5 is the inherent resolution of the matched filter. Smaller sub-band width results in larger processing bins (resolution), yielding significantly reduced time delay (range) precision. As the processing time is increased, finer details may be able to be resolved.

B. Echo Width

Although larger processing bands allow for resolving finer details in the correlation, if the peak width of the echo correlation is wider than the cell resolution, then the expected detection and ranging performance will not be realized; this is known as the effect of energy splitting loss (ESL). The underlying width of the peaks are theoretically proportional to the inverse of the bandwidth processed (as in Eq. 4), however several effects can contribute to temporally spread a target echo beyond this. The narrowing of the peaks will continue with increasing bandwidth until other sources of spreading dominate, at which point no more pulse compression can be achieved with additional bandwidth. One or more of the following spreading effects may contribute to ESL.

- A target may have non-negligible dimensions (range-extent) which will produce echo spread corresponding to the target's length and presented aspect angle.
- If Doppler-matched processing is not performed, target motion within the processing interval will produce echo spread corresponding to the target's change in range, limiting the performance as processing time increases. This effect can be mitigated by performing Doppler-matched processing over the range of all hypothesized target speeds.
- Underwater acoustic channels spread target echoes due to multipath propagation coming from sound refraction and boundary interactions. This is particularly a problem for shallow water environments.

Fig. 7 shows a notional representation of these spreading terms (for a point target) in order to visualize the trends of each component and their result on the total. The bandwidth spreading is proportional to $1/B_p$, Doppler is a scalar factor times the processing time, and the Environmental term is represented as a constant (though in reality, there may be some frequency dependence of this). These effects can be observed for the peaks shown in Fig. 5; for the Doppler-mismatched targets, the Doppler spreading begins to dominate for T_p from 4-9 sec.

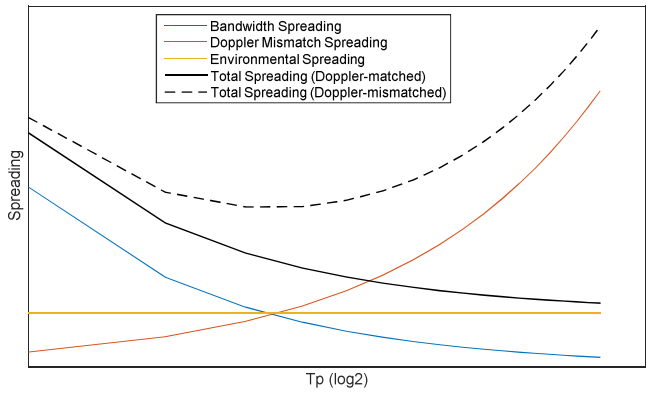

Fig. 7. Notional representation of spreading terms: bandwidth, mismatched Doppler, and environmental. Total spreading is sum of curves (both including and excluding Doppler).

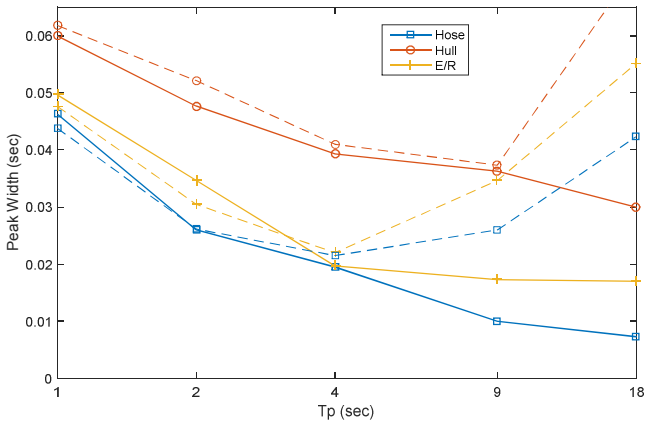

Fig. 8. Echo peak width; solid lines are matched Doppler (0 kts for Hose, 5 kts for Hull and E/R); dashed lines are mismatched Doppler.

To obtain statistical results of peak spreading, echo widths were calculated by hand for detections on the three targets in six selected scans by measuring the peak width at a point 6 dB below the maximum value of the peak. Averages of the peak widths across the six scans for each of the targets for both Doppler-matched and mismatched replicas are shown in Fig. 8 as functions of processing time (bandwidth). The results are consistent with the expected trends described above. It is observed that the two point-like targets (Hose and E/R) are narrower for all T_p than the Hull due to the fact that the Hull has additional spreading due to the physical extent of the ship. Also, the peak widths for these two targets decreases by close to the expected factor of two for each doubling of bandwidth until about T_p = 4 sec, at which point they level off, indicating the point at which other spreading terms begin to dominate; the Hull does not decrease as much per doubling of bandwidth due to the additional target spreading. The Doppler-matched and mismatched cases are nearly identical until T_p=4, where the Doppler spreading begins to dominate.

C. Receive Levels

The pre-normalized receive levels for all contacts formed on the E/R via the automated processing are shown for six

different processing lengths in Fig. 9. The receive level drops over time as the target moves further away. It is also observed that the average signal level decreases with increasing T_p. In a theoretical (non-spread) environment, there would be no loss in signal level with increasing T_p, and thus the linear fit lines would lie directly on top of each other. However, due to the incoherence of the channel in both time and frequency, energy spreading is introduced; energy splitting losses are introduced as the echo energy is distributed across multiple observation cells. For the TREX data, time spread is observed to have standard deviation of ~0.012 seconds [9]. This is not a huge time spread, and results because the environment is extremely shallow constraining most paths to arrive similarly in time and any reflected paths (with steeper angles) quickly attenuate due to many multiple surface/bottom interactions. The detector losses attributable to such spreading can be predicted using the Bell-Jones ESL model [10].

Fig. 10 shows the peak correlation levels for the three targets, averaged over all scans for each T_p. The peak level losses can be more clearly seen and calculated to be between 1.5 and 2 dB per doubling of T_p for the shorter processing times, but with their rate of descent increasing at the longer

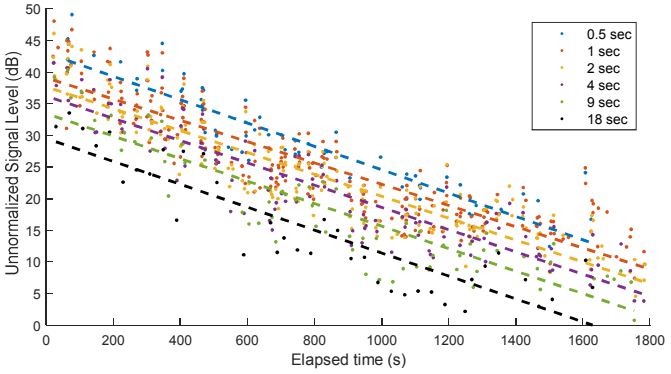

Fig. 9. Pre-normalized signal receive levels of all contacts for six processing tims over duration of run; linear trend lines shown dashed.

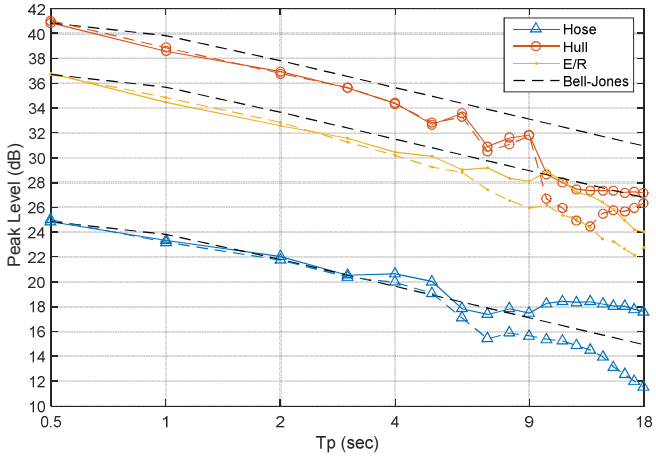

Fig. 10. Relative peak levels for three targets for Doppler-matched (solid) and mismatched (dashed) from automated processing (averaged over all contacts).

processing times, showing drops of approximately 3 dB from 9 to 18 sec. This agrees with the ESL predicted by the Bell-Jones model, shown in dashed black lines. The ESL has been normalized to the first data point (T_p = 0.5) for each target to show the relative losses between them as T_p is increased. In addition, it is once again observed that the losses due to Doppler mismatch are negligible until approximately T_p=4, at which point they become significant.

D. SNR

As already discussed in section III, each doubling of processing time should theoretically result in a 3 dB processing gain against noise, while each doubling of processed bandwidth corresponds to a 3 dB processing gain against reverberation. Thus, since T_p and B_p are directly linked in an LFM waveform, and because of the matched filter convention to maintain constant peak level, each doubling of processing time should result in a 3 dB decrease in background level regardless of whether it is noise- or reverb-limited. Fig. 11 shows a moving average trend (1001 sample window length) of the correlations for the 5 different sub-bands. As expected, we see, on average, a 3 dB reduction in background level with each doubling of processing time. The left plot in Fig. 12 shows SNR as a function of processing time for the three targets, with the right plot showing the change in SNR relative to the first point (T_p=1 sec).

According to theory, in a perfect environment, we would expect to see a 3 dB increase for each doubling of T_p due to the 3 dB decrease in background level just presented. However, due to the ESL, the gain we observe is less than the theoretical 3 dB, and averages between 1.5, as observed on the Hull, and 2 dB, as observed on the Hose and E/R. We note that the overall SNR of the Hull is highest but also provides the lowest improvement per doubling of processing time. This is due to the additional spreading losses incurred due to the target extent of the Quest.

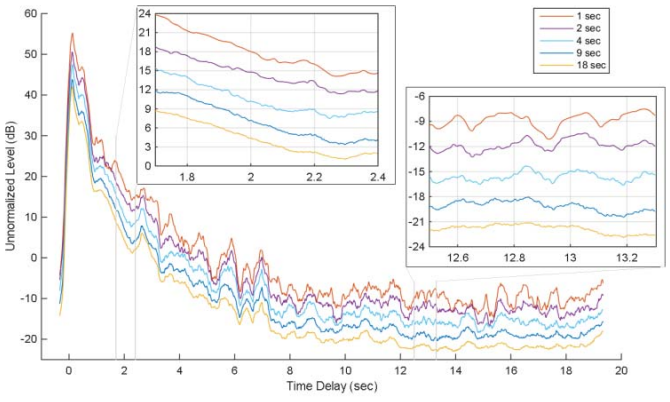

Fig. 11. Background levels of one transmission cycle showing both reverb- and noise-limited regions.

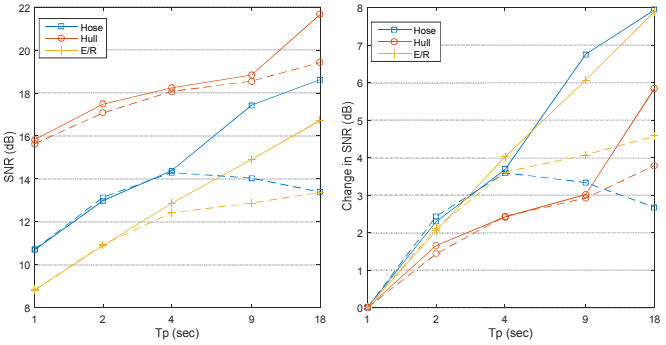

Fig. 12. SNR as a function of processing time (left); change in SNR (right); Doppler matched (solid), Doppler mismatched (dashed).

E. *Doppler Effects*

Fig. 13 shows cross-sections of the ambiguity surfaces presented in Fig. 3 at various Doppler offsets (different colored sets of peaks). For each Doppler offset, the 5 different processing times (1 through 18) are shown. This provides a comprehensive view of the three consequences of Doppler mismatch (increased peak width, reduced peak amplitude, and increased bias) as the mismatch increases as well as in relation to T_p. At zero Doppler mismatch (purple curves), the peak widths continue to get narrower by a factor of two for each doubling of T_p. However, at 5 kt mismatch, we observe a different trend: the peak width decreases only until T_p = 4, and then the peaks become wider again. This is because the inherent resolution of the correlation is wider than the Doppler spreading until T_p = 4. At this point, the Doppler spread begins to dominate and the peak width increases (the fanning effect observed in Fig. 3). This effect can also be observed in Fig. 5, where in the left column, the peak widths of the Hull and E/R get narrower, and then begin to widen again, and likewise for the Hose peaks in the right hand column.

The reduced peak amplitude due to Doppler mismatch follows a similar trend. As already observed in Figs. 10 and 12, the received levels are approximately the same between Dopplerized and unadjusted replicas up through about T_p = 4 sec. With longer replicas however, we begin to see an accelerated rate of reduction in received peak level and

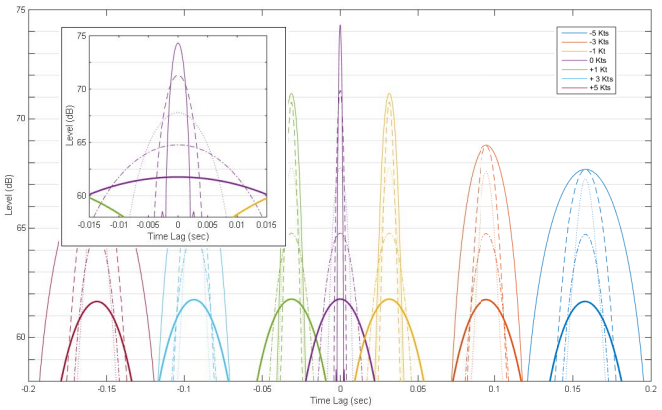

Fig. 13. Ambiguity function vs. Doppler offset and processing interval.

reduction in SNR as compared to the Doppler-matched replicas. The reason for this can be seen in Fig. 13. We observe the expected 3 dB of increase in peak level when perfectly Doppler-matched. However, with a 1 kt mismatch, we only see increases from T_p = 1 through 9, with T_p = 18 providing almost no improvement. At a 5 kt mismatch, we see that there is still no peak loss for T_p = 1 and 2, and but we now observe only a 2.5 dB gain for T_p = 4, and almost no gain for T_p = 9 and 18. We see that for small processing times (T_p = 1-2 sec) there is no degradation due to Doppler mismatch.

The bias error is the only effect of the three that is not processing time dependent. This was observed in the ambiguity surfaces by the identical slopes for all processing times. It is determined by the amount of Doppler mismatch in relation to the slope rate of the waveform. For the configuration used in this dataset there is an expected bias of approximately 0.158 sec at 5 kts for a replica centered in the transmitted sweep at 2250 Hz.

As mentioned earlier, this bias error between non-Doppler and Doppler processing in Fig. 5 is not apparent due to the way that processing was done. For the non-Doppler replica, all 5-knot target echoes are biased to the right. Conversely, for the Dopplerized replica, all fixed target echoes are biased to the left. This is shown in Fig. 14, where the left plot has been processed with a 0-knot replica and has been aligned such that 0-knot targets are correctly located, and the right plot is for a 5-knot replica and aligned for 5-knot target contacts. The A-scans shown in Fig. 5 are plotted such that fixed target peaks (Hose) are at the correct time offset regardless of which waveform was used, and the moving targets (Hull and E/R) are biased to the right. Additionally, we observe that with the 0 kt replica there is a sawtooth pattern to the contacts from the mobile targets (Hull and E/R) and vice versa for the 5 kt replica and the fixed Hose. The contacts shown are for the 1-sec replica, and thus there are up to 18 contacts per transmitted sweep. The higher frequency sub-bands have a larger bias than the lower frequency sub-bands, creating the sawtooth pattern, as mentioned in section IV.

Fig. 15 shows A-scans of scan 26 for the case where the bias has not been adjusted for. The offset between the E/R and Hose echoes for the two processing methods are measured to be 0.153 and 0.160 sec, respectively, which agrees closely to the anticipated value of 0.158 listed earlier. In order to achieve a "correct" scan for both targets, the blue portion would need

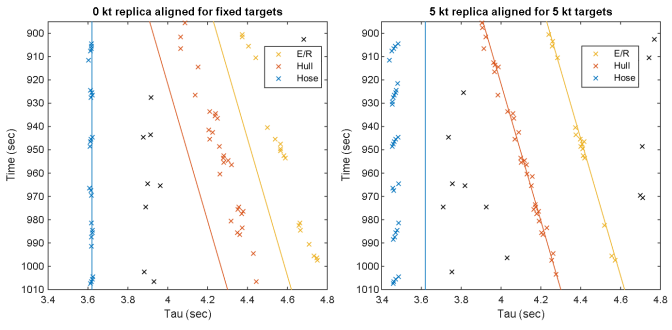

Fig. 14. Matched filter processed to remove bias of stationary targets (left) and moving targets (right)

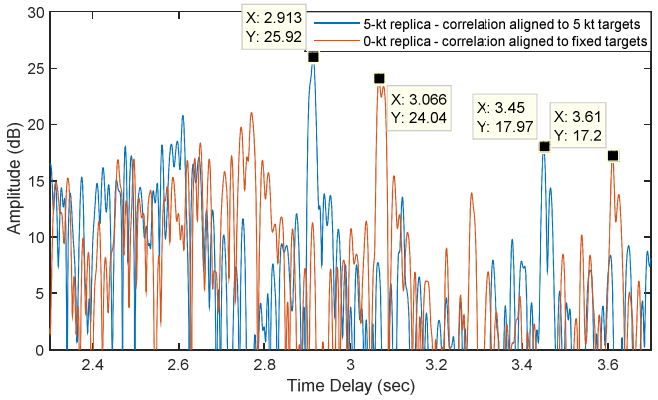

Fig. 15. Correlation peaks exhibiting Doppler-induced range-bias errors.

to be chosen for the mobile targets and spliced with the red potion for the fixed targets. Correction for this bias error in the case of targets with unknown Doppler can be applied in one of two ways. The direct method would be to process a bank of matched filters, each with a different Dopplerized replica. Contacts would then need to be clustered in such a way so as to only pull detections from the correct Doppler slice. Alternatively, the approach described in [6] is capable of estimating Doppler from detections using a mismatched replica. This is computationally more efficient, but will only work if sufficient signal excess exists to pull out detections that suffer from SNR loss due to Doppler mismatch, as described earlier.

F. Signal shading effects

For PAS (or full band HDC) sonar, the transmitted pulse is typically shaded. For HDC sonar, an unshaded transmission is most conducive to sub-band processing, as has been implemented in the TREX trial. However, even for the case of an unshaded transmission, it is very important that the correlation replica is shaded in the receive processing to avoid significant sidelobe leakage. Fig. 16 shows a simulated LFM waveform correlated with both an unshaded and a Hanning-shaded replica for the 4-second, centered sub-band (2150-2350 Hz). There are three main factors we can observe. The primary one is the significantly lower sidelobes for the Hanning-shaded correlations. In addition, there is a slight decrease in peak level for both Doppler cases, with the reduction on the Doppler-matched case being more significant. This effectively reduces the sensitivity of the waveform to Doppler mismatch in terms of peak amplitude. The third effect is a slight widening of the peaks, as a necessary trade-off of windowing in exchange for the lower sidelobes. Although the shaded Doppler-mismatched peak appears narrower, this is due to the sidelobes extending very high and adjacent to the main peak for the unshaded case. For the larger sub-bands, the Doppler-mismatched correlation would exhibit an even further reduced peak height (-25 dB for the full band) and increased peak width, as shown in the previous discussions.

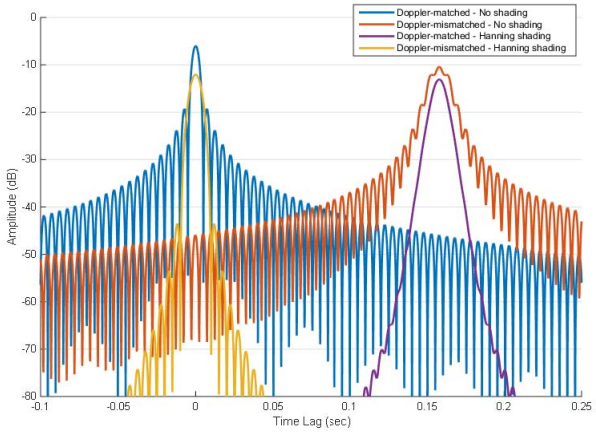

Fig. 16. Correlation of Hanning-shaded and non-shaded replicas for $T_p = 4$.

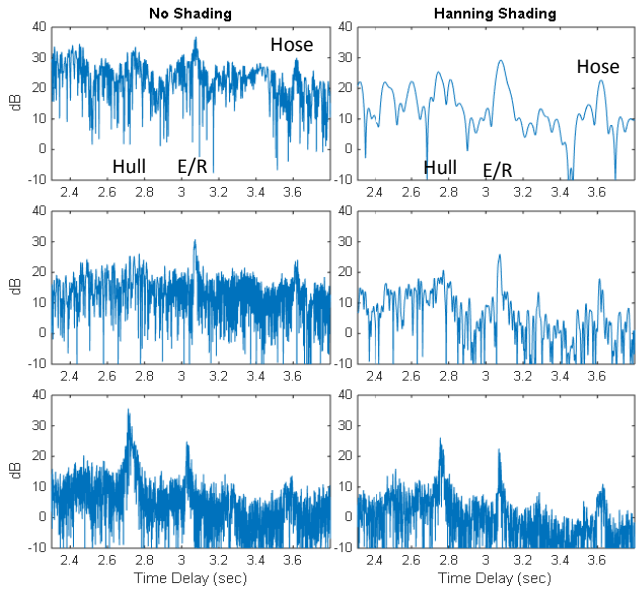

Fig. 17. Correlations for T_p = 1, 4, and 18 sec for non-shaded (left) and Hanning shaded (right) replicas of scan 26 of the TREX data.

The result of this sidelobe interference is observed in the TREX data in Fig. 17. Here we see that the left hand plots demonstrate noisy correlation peaks due to the sidelobe interference. The interference also results in a higher background "noise" floor, obscuring lower peaks. The reduced peak levels due to windowing are clearly observed in the right hand plots, but this tradeoff is worth the reduced background level, resulting in a higher overall SNR and better detectability.

G. Frequency dependencies

An additional complication in selecting sub-band size in HDC sonar is that not all sub-bands will necessarily have the same performance. Since each sub-band is comprised of a unique frequency band, any frequency response of the environment and/or target object will affect the detection performance of that band. To estimate what, if any, frequency dependence existed, the probability of detection (PD) was

computed for all 50 Hz sub-bands within the 1800-2700 Hz range (18 different sub-bands, sub-band #1 corresponding to the lowest frequency and sub-band #18 to the highest). The results are shown in Fig. 18. For each sub-band, the number of detections for the entire run was divided by the number of detection opportunities (scans). Because the E/R only produced an echo every other ping, its number of detection opportunities were half the number of scans as for the Hull or Hose. PD was computed for a range of detection thresholds in order to verify that the trends were consistent.

The three targets exhibit a different frequency responses. The E/R is the flattest, with little trend to be observed amongst the sub-bands, indicating that there is not a significant variation due to the acoustic environment. The physical shapes of the Hull and Hose, however, result in spectral coloration, with the Hull demonstrating a significant peak towards the higher sub-bands, and the Hose having two peaks in the middle of the range.

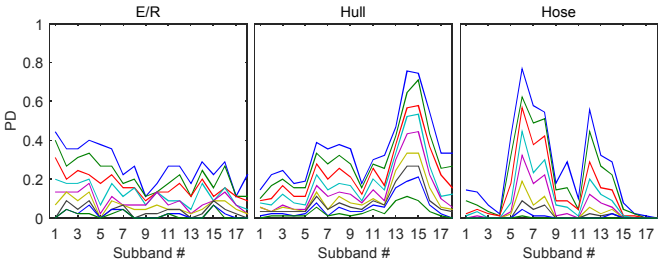

Fig. 18. PD for 50 Hz sub-bands vs. sub-band number (from 1825 to 2675 Hz center frequency, and vs (various colored) detection thresholds.

VII. Summary and Conclusions

A new parameter introduced with HDC sonar is the choice of processing interval and its corresponding sub-bandwidth. The objective of this paper was to highlight some of the factors that will influence the choice of this parameter. A key advantage of HDC sonar is the possibility of getting more detection opportunities per ping repetition cycle, thereby improving target tracking, localization, and holding performance. On the other hand, one may be naturally inclined to utilize as much of the additional signal time-bandwidth that HDC provides (due to the extended duration of the pulse) as possible, to achieve all possible pulse compression gains. However, in doing this, the expected gains may not be completely available and it will cost additional detection opportunities that HDC is designed to provide. If there is sufficient signal excess, many lower PD detection opportunities are preferred over a few higher PD opportunities.

As processing time/bandwidth increases, noise and reverberation rejection improves, yet the system will still be subject to energy splitting losses. The effect of the environment, the target's physical extent, and its motion (when Doppler-matching processing is not implemented), will all spread the target echo and subject the sonar to signal losses and limit ranging accuracy (resolution and bias). Additional processing bandwidth/time beyond these limits will not provide the expected gains. This was shown with the TREX data, for extended vs. compact targets and fixed vs. mobile targets in a real acoustic environment. Also, the impact of Doppler processing (or lack of it) on HDC signals was shown. Doppler mismatch between replica and target echo may be negligible for short processing times, but for longer (or fullband) processing they can produce significant degradations. It was shown that HDC receiver processing should always include shading to reduce the effect of strong direct blast transmission leaking into sidelobes and obscuring potential target detections.

The choice of processing time/bandwidth is best made by understanding the predicted sonar performance, the various expected spreading effects and considering the tactical advantages of rapid detection revisit rate (i.e., localization vs. detection). It was shown that frequency dependencies may need to be understood as well.

Acknowledgment

We acknowledge Dr. Paul Hines, Mr. Jeff Scrutton, and Mr. Stefan Murphy of Defence R&D Canada-Atlantic who designed and conducted the TREX'13 experiment; Dr. Dajun Tang, Dr. Todd Hefner, and Dr. Kevin Williams of the Applied Physics Laboratory of the University of Washington who managed and led the TREX'13 trial, and Dr. John Preston of Penn State University's Applied Research Lab who managed quality control and data collection for the experiment. We wish to acknowledge the officers and crew aboard CFAV QUEST and RV SHARP, and the APL-UW dive team for their support throughout the trial. Funding for this work was provided by ONR Code 32 and ONR Global-London.

References

[1] D. Grimmett, Multistatic sensor placement with the complementary use of Doppler sensitive and insensitive waveforms, NURC Technical Report SR-427, July, 2004

[2] G. Hickman, J. Krolik, Non-recurrent wideband continuous active sonar, in proceedings IEEE OCEANS'12, Hampton Roads, VA, October 2012.

[3] D. Grimmett, C. Wakayama, Multistatic Tracking for Continous Active Sonar using Doppler-Bearing Measurements, Proceedings 16th Int. Conference on Information Fusion, July, 2013, Istanbul, Turkey.

[4] D. J. Grimmett, Target AOU Growth Containment using LFM High Duty Cycle Sonar, *in Proceedings of the 2nd International Conference on Underwater Acoustics*, June, 2014, Rhodes, Greece.

[5] X. Song, P. Willet, S. Zhou, Posterior Cramer-Rao Bounds for Doppler biased Multistatic Range-only Tracking, Proceedings 14th International Conference on Information Fusion, Chicago, U.S.A., July 2011.

[6] D. J. Grimmett, Target Doppler Estimation and Range Bias Compensation using LFM High Duty Cycle Sonar, *in Proceedings of the 2nd International Conference on Underwater Acoustics*, June, 2014, Rhodes, Greece.

[7] A. A. Winder, "II. Sonar System Technology", IEEE Trans. Sonics and Ultrasonics, Vol SU-22, No. 5, September 1975.

[8] P. Hines, Experimental Comparison of Continuous Active Sonars in Littoral Waters, in proceedings 1st Underwatr Acoustics Conference and Exhibition, Cofu, Greece, June 2013.

[9] D. A. Abraham, CausaSci LLC, personal communication, 2014.

[10] R.P. Hodges, "Underwater Acoustics", Wiley: West Sussex, 2010, pp. 250-251